Structural Perturbations in Human ADP Ribosylation Factor−1 Accompanying the Binding of Phosphatidylinositides †

ARTICLE *in* BIOCHEMISTRY · JANUARY 2005

Impact Factor: 3.02 · DOI: 10.1021/bi0490385 · Source: PubMed

4 AUTHORS, INCLUDING:

Richard A Kahn
Emory University
170 PUBLICATIONS **9,906** CITATIONS

THE JOURNAL OF BIOLOGICAL CHEMISTRY
Vol. 279, No. 46, Issue of November 12, pp. 48307–48318, 2004
Printed in U.S.A.

Conformational Changes in Human Arf1 on Nucleotide Exchange and Deletion of Membrane-binding Elements*[S]

Received for publication, February 25, 2004, and in revised form, August 6, 2004
Published, JBC Papers in Press, August 12, 2004, DOI 10.1074/jbc.M402109200

Ronald D. Seidel III‡, Juan Carlos Amor§, Richard A. Kahn§, and James H. Prestegard‡¶

From the ‡Complex Carbohydrate Research Center, University of Georgia, Athens, Georgia 30602-4712 and the §Department of Biochemistry, Emory University School of Medicine, Atlanta, Georgia 30322-3050

Conformational changes associated with nucleotide exchange or truncation of the N-terminal α-helix of human Arf1 have been investigated by using forms of easily acquired NMR data, including residual dipolar couplings and amide proton exchange rates. ADP-ribosylation factors (Arfs) are 21-kDa GTPases that regulate aspects of membrane traffic in all eukaryotic cells. An essential component of the biological actions of Arfs is their ability to reversibly bind to membranes, a process that involves exposure of the myristoylated N-terminal amphipathic α-helix upon activation and GTP binding. Deletion of this helix results in a protein, termed Δ17Arf1, that has a reduced affinity for GDP and the ability to bind GTP in the absence of lipids or detergents. Previous studies, comparing crystal structures for Arf1·GDP and Δ17Arf1·GTP, identified several regions of structural variation and suggested that these be associated with nucleotide exchange rather than removal of the N-terminal helix. However, separation of conformational changes because of nucleotide binding and N-terminal truncation cannot be addressed in comparing these structures, because both the bound nucleotide and the N terminus differ. Resolving the two effects is important as any structural changes involving the N terminus may represent membrane-mediated conformational adjustments that precede GTP binding. Results from NMR experiments presented here on Arf1·GDP and Δ17Arf1·GDP in solution reveal substantial structural differences that can only be associated with N-terminal truncation.

ADP-ribosylation factors (Arfs)[1] comprise a family of 21-kDa GTPases ubiquitously expressed in eukaryotic cells. The six mammalian Arf proteins regulate a wide variety of intracellular signaling pathways, particularly those impacting bi-directional membrane traffic at the Golgi, trans-Golgi network, and the plasma membrane. Essential components of the action of Arfs *in vivo* are the abilities to reversibly bind to membranes, to activate lipid-modifying enzyme activities (*e.g.* phospholipase D or PI(4)P 5-kinase) (1–3), and to recruit or stabilize the binding of other proteins to those same membranes; prominent among the latter are coat proteins, including COPI, GGAs, adaptins, and MINTs (4–7). Membrane binding of ARF is controlled by exposure of a myristoylated, N-terminal α-helix upon exchange of GDP for GTP. Although the changes in protein structure that accompany nucleotide exchange are critical aspects of all regulatory GTPases, they are particularly important to Arfs, which directly couple the activation process to membrane translocation (8–10). Indeed, the formation of activated Arf on a membrane surface is viewed as the initial event that nucleates the formation of a coated bud and subsequent coated vesicle. Biochemical information pairing the nucleotide binding cycle to membrane interactions provides evidence for this pivotal role of the N-terminal helix and attached acyl chain. We present here structural data relevant to this process.

Current proposed mechanisms whereby both the myristoyl chain and the N-terminal helix are exposed are based on a detailed comparison of the full-length, nonmyristoylated, and GDP-bound x-ray crystal structure (later referred to as Arf1·GDP) (11) to other nonmyristoylated structures. Specifically, a truncated form of Arf1 lacks both the N-terminal helix and the myristoyl chain and is bound to a nonhydrolyzable GTP analog Gpp(NH)p (later referred to as Δ17Arf1·GTP); a truncated apoArf form lacks nucleotides as well as the terminal helix that is bound to the catalytic Sec 7 homology domain of the guanine nucleotide exchange factor Gea2 (8).

Structurally Arfs, as represented in the Arf1·GDP crystal structure (11) (Fig. 1*A*), consist of a mixed parallel/antiparallel 6 β-strand core surrounded by 6 α-helices and 12 connecting loops. Residues 2–17 constitute the aforementioned N-terminal, amphipathic α-helix (αNt) and flexible connecting loop region (L_{Nt}, found adjacent to αNt, not labeled, however). The myristoyl chain, when present, is attached at residue 2, the N-terminal glycine (11–14). The N-terminal helix as a whole lies in a cleft parallel to the C-terminal helix (αCt) located on the side of the protein opposite the nucleotide-binding site (8, 15, 16). The residues involved in nucleotide binding include and are labeled as phosphate-binding loop residues (P-loop, residues 26–30) and the guanine base-binding motif (G3Motif, residues 126, 127, and 129). Connecting the nucleotide-binding site and the N-terminal helix are distinctive switch regions (termed SW1, SW2, and the inter-switch by analogy to Ras proteins (17–19)). These change conformation in response to the bound nucleotide. Switch 1 (SW1, residues 42–54), forms a seventh β-strand at the periphery of β2 in Arf1·GDP. Addition-

* This work is supported by the National Institutes of Health Grant GM61268. The costs of publication of this article were defrayed in part by the payment of page charges. This article must therefore be hereby marked "*advertisement*" in accordance with 18 U.S.C. Section 1734 solely to indicate this fact.

[S] The on-line version of this article (available at http://www.jbc.org) contains measured RDCs and additional text.

The atomic coordinates and structure factors (code 1U81) have been deposited in the Protein Data Bank, Research Collaboratory for Structural Bioinformatics, Rutgers University, New Brunswick, NJ (http://www.rcsb.org/).

¶ To whom correspondence should be addressed: Complex Carbohydrate Research Center, University of Georgia, 315 Riverbend Rd., Athens, GA 30602-4712. E-mail: jpresteg@ccrc.uga.edu.

[1] The abbreviations used are: Arfs, ADP-ribosylation factors; RDCs, residual dipolar couplings; NOE, nuclear Overhauser effect; NOESY, nuclear Overhauser effect spectroscopy; r.m.s., root mean square; r.m.s.d., root mean square deviation; RT, room temperature; HSQC, heteronuclear single quantum coherence; C_8E_5, pentaethylene glycol octyl ether; PI, phosphatidylinositol; MOPS, 4-morpholinepropanesulfonic acid; Amp, ampicillin; αNt, N-terminal α-helix; αCt, C-terminal helix.

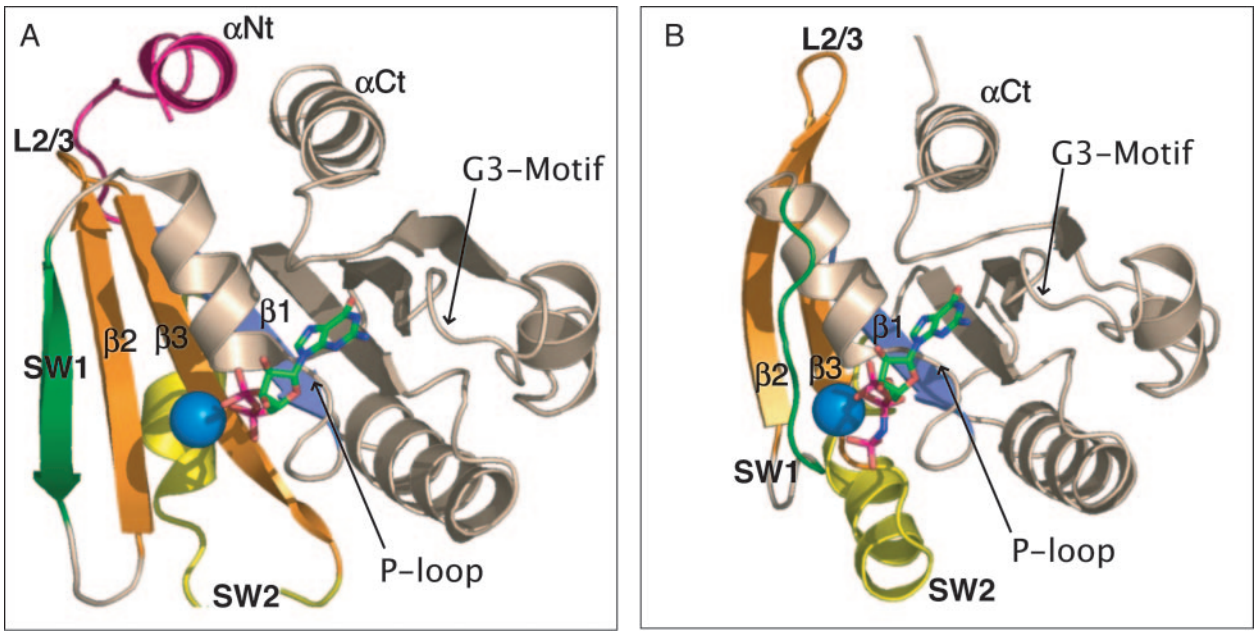

FIG. 1. **Important structural features of Arf1·GDP (1HUR (11)) (*A*) and Δ17Arf1·GTP (8) (*B*).** Regions having the lowest degree of structural variation (r.m.s.d. of overlaid structures being 0.3 Å) are shown in *neutral tones*. Highly variable regions are labeled and color-coded as follows: αNt (residues 2–17), *magenta*; switch 1 (42–52), *green*; Inter-Switch β2-β3 (53–68), *orange*; and switch 2 (70–85), *yellow*. Figure was generated by using the PyMol Molecular Graphics System (44).

ally, residues 70–85 referred to as switch 2 (SW2) have been suggested to undergo a transition from an extended loop to a more ordered helical segment as a result of nucleotide exchange (1). Finally, the inter-switch β-strands (ISR, defined as β2, β3, and $L_{2/3}$ (residues 51–68)), undergoing the largest degree of observed conformational change, are displaced by 7 Å, thus allowing for occupation of the cleft used for binding the N-terminal helix, vacated upon the N-terminal helix release (20).

As Δ17Arf1·GTP differs from Arf1·GDP with respect to both the N-terminal helix and the bound nucleotide, it is difficult to differentiate changes associated with nucleotide exchange and truncation. In solution it is possible to examine a third form of Arf1, Δ17Arf1·GDP, which allows for separation of these associated changes by direct comparison to crystal structures differing in nucleotide (Δ17Arf1·GTP) and differing by truncation (Arf1·GDP). We have carried out this examination by using chemical shift perturbations of heteronuclear single quantum coherence (HSQC) spectra, changes in amide proton exchange rates, and residual dipolar couplings (RDCs), all collected from NMR data on a ^{15}N-labeled form of the protein. In particular, measured residual dipolar couplings from Δ17Arf1·GDP, along with calculated values from the crystal structures of Arf1·GDP and Δ17Arf1·GTP, have allowed production of a structural model for Δ17Arf1·GDP and have made it possible to discern which changes are likely to be a direct result of nucleotide exchange as opposed to those derived from truncation.

Residual dipolar couplings arise from a through-space interaction between pairs of magnetic nuclei. They are easily observed in ^{15}N-labeled proteins as additional contributions to splittings of amide nitrogen-amide proton cross-peaks in HSQC experiments when proteins are oriented in field-ordered liquid crystals. The contributions are dependent both on the distance (r) between the nuclei and the angle (θ) between the internuclear vector and the magnetic field. When the distance is fixed, as in a directly bonded pair, the splitting of the NMR resonances for the two nuclei, i and j, due to residual dipolar coupling is given by Equation 1.

$$D^{ij}_{\mathrm{RES}} = D^{ij}_{\max} \langle (3\cos^2\theta - 1)/2 \rangle \qquad \text{(Eq. 1)}$$

Here $D^{ij}_{\max}$ is the dipolar coupling between the nuclei in a perfectly ordered system with $\theta = 0$. Averaging over allowed orientations, as denoted by the parentheses, greatly reduces the observed values, but the residual values can be analyzed to provide both structural information and the nature of molecular order when sufficient measurements can be made (21, 22). The structural information is complementary to distance constraints normally derived from ^{1}H-^{1}H NOEs but can also be used independently when suitable starting structures are available. In cases where structural homology is considered high, incorporation of constraints on individual bond vector orientations as penalty functions in refinement processes can result in the generation of model structures from experimental data.

Penalty functions require the back calculation of RDCs from the coordinates of bond vectors in trial structures. These couplings can be expressed in terms of direction cosines, $\cos\theta^{ij}_k$, relating various interaction vectors, ij, to the axes, k, of an arbitrarily chosen fragment frame as shown in Equation 2.

$$D^{ij} = D^{ij}_{\max} \sum S_{kl} \cos\theta^{ij}_k \cos\theta^{ij}_l \qquad \text{(Eq. 2)}$$

Here the degree of order within the system is represented by the molecular order parameters S_{kl}. These form a traceless symmetric matrix that allows only five of the order parameters to be independent. When RDCs can be measured for a sufficient number of vectors within a rigid molecular fragment (a conserved portion of a protein structure), a complete evaluation of the elements of the order matrix can be achieved. The independent order parameters can be translated into Euler angles needed to rotate the molecule into a principal alignment frame where the two remaining parameters can be associated with the principal order parameter in this new frame, S'_{zz}, and the asymmetry of order in this frame, $\eta = (S'_{yy} - S'_{xx})/S'_{zz}$.

In the following, we propose a solution structure of Δ17Arf1·GDP derived by incorporation of RDC-associated penalty functions into an energy minimization protocol. We use this structure to assess regions of Δ17Arf1·GDP that deviate when compared with both the Arf1·GDP and Δ17Arf1·GTP crystal structures. The former comparison identifies structural

differences that can be associated with N-terminal truncation, and the latter comparison identifies differences that can be associated with nucleotide exchange. The differences are supported by a limited set of NOE data in some critical aspects of the structure. Additional data showing differences in amide exchange rates between full-length Arf1·GDP and Δ17Arf1·GDP also highlight subtle changes in the nucleotide-binding pocket that may be responsible for the alteration in relative affinities for GDP and GTP on truncation.

EXPERIMENTAL PROCEDURES

Sample Preparation—BL21(DE3) cells were transformed with the expression plasmid for Δ17Arf1 (pOW14) or Arf1 (pOW12), respectively, in media containing 60 μg/ml ampicillin incubated at 37 °C. Both sets of transformed cells were grown in 3 ml of LB/Amp to saturation, collected, and placed in 50 ml of LB/Amp and grown to an A_{600} of 0.6. Cells were collected, resuspended, and added to 1 liter of MOPS/Amp media (23), supplemented with 1× of vitamin mix (Invitrogen, catalog number 11120-052), adding 1 g/liter $^{15}NH_4Cl$ and 2 g/liter [$^{13}C_6$]glucose (Cambridge Isotope Laboratories) (Δ17Arf1) or 4 g/liter glucose (Arf1). Protein expression was initiated by the addition of isopropyl 1-thio-β-D-galactopyranoside to 0.5 mM (at A_{600} of 1.0) and incubated for an additional 3–5 h. Cells were resuspended in 10 ml of TM buffer (20 mM Tris, 2 mM $MgCl_2$, pH 7.6, at room temperature (RT)), broken using a French press at 20–25,000 pounds/square inch, and subsequently clarified by centrifugation (100,000 × *g*, 1 h).

Proteins were purified in two chromatographic steps. The first step was by using a 50-ml Q resin column (Bio-Rad, Q-macro, high substitution) equilibrated in TM buffer (20 mM Tris, 2 mM $MgCl_2$, pH 7.6, at RT) and resolved with a 20% gradient of TMN buffer (containing 1 M NaCl). In the second step proteins were pooled and concentrated to 0.5 ml and loaded onto a 60-cm, 120-ml Superdex-75 column (Amersham Biosciences) and resolved at 1.0 ml/min with phosphate buffer (10 mM KPO_4, 50 mM NaCl, 1 mM $MgCl_2$, and 5 mM NaN_3, pH 7.0, at RT).

Nucleotide exchange on Δ17Arf1 was achieved by incubating the protein with a 50- or 10-fold molar excess of GDP or GTP (not an analog), respectively, including 10 mM EDTA and incubating the reaction either overnight at RT for GDP or for 60 min at RT for GTP. Exchange reactions were quenched by addition of 30 mM $MgCl_2$. Excess nucleotide, EDTA, and $MgCl_2$ were removed by chromatography on a Superdex-75 column using phosphate buffer. Protein-containing fractions were pooled and concentrated to a final concentration of 1 mM.

Samples used for triple resonance assignment (Δ17Arf1·GDP) and HSQC-NOESY experiments (Δ17Arf1·GDP and Arf1·GDP) contained 0.5 mM protein in potassium phosphate buffer (mentioned above) with 10% ^2H_2O added to provide a lock signal. The samples for measurement of residual dipolar couplings were prepared as follows. Arf1·GDP was prepared to be 0.5 mM protein in the aforementioned phosphate buffer with 10% ^2H_2O added to provide a lock signal. The 7% (w/v) bicelle solution contained dimyristoylphosphatidylcholine/dihexanoylphosphatidylcholine at a 2.8:1 molar ratio doped with dimyristoylphosphoglycerol (15:1 dimyristoylphosphatidylcholine/dimyristoylphosphoglycerol). This gave a 13.8-Hz splitting of the ^2H NMR signal from 10% ^2H_2O in the sample at 305 K. The sample of Δ17Arf1·GDP was prepared to be 0.5 mM protein, again in the aforementioned phosphate buffer. The 7.5% (w/v) ether bicelle solution contained 1,2-di-*O*-tetradecyl-*sn*-glycero-3-phosphocholine/1,2-di-*O*-hexyl-*sn*-glycero-3-phosphocholine (Avanti Polar Lipids, Alabaster, AL) at a 3:1 molar ratio. This gave a 15-Hz splitting of the ^2H NMR signal from 10% ^2H_2O in the sample at 303 K. A similar sample using 4% pentaethylene glycol octyl ether (C_8E_5):octanol (Sigma) having a molar ratio (*r*) of 1.01, as an alignment medium, was used for additional measurements of dipolar couplings on Δ17Arf1·GDP. The C_8E_5:octanol system yielded a 14-Hz splitting of the ^2H NMR signal from 10% ^2H_2O present in the sample buffer at 301 K.

Due to the heightened affinity for nucleotide triphosphates in truncated Arf1 samples, an assessment of possible contamination from GTP incorporation into the target protein (Δ17Arf1·GDP) was performed. GDP and GTP have distinctive ^{31}P chemical shift values, also reflecting the coordination of Mg^{2+} when present and allowing for a direct detection of bound nucleotide by observation of phosphorous atoms in the nucleotide itself. The results show Mg^{2+}-coordinated GDP as the bound nucleotide with GDP and trace amounts of inorganic phosphate and GMP found in solution (Table I). Comparing integrated peak intensities of ^{31}P peaks observed in the spectra from GDP to internal standards (inorganic phosphate from sample buffer) indicates greater than 85% occupation of the nucleotide-binding pocket.

TABLE I
^{31}P chemical shift values from Arf samples

	α	β	γ	P_i
Δ17GDP	−9.561	−3.612	[a]	2.15
Δ 17GDP −(Mg)	−9.63	−4.34	[a]	[b]
Free GDP	−10.7	−6.3	[a]	2.2
Δ 17GTP	−9.4	−15.1	−4.8	2.12

[a] No γ-phosphate present.
[b] Succinate buffer used; therefore, no inorganic phosphate was detected from the buffer.

NMR Spectroscopy—Spectra for the heteronuclear triple resonance assignment experiments, as well as the coupled in-phase anti-phase ^1H-^{15}N HSQC experiments used to measure residual dipolar couplings, were collected on Varian 800- and 600-MHz spectrometers, respectively, using Z-gradient triple resonance probes (Varian Inc., Palo Alto, CA). Heteronuclear three-dimensional experiments (including HNCA, HNCACB, CBCACONH, HNCO, and HN(CO)CA) were run at 298 K using standard gradient-assisted pulse sequences as supplied as part of the Varian protein pack. In addition a ^{15}N-edited TOCSY experiment (24, 25) provided assignment of most α-proton resonances.

^{15}N-Edited ^1H-^1H HSQC-NOESY experiments were collected on a Varian 600-MHz spectrometer using a Z-gradient triple resonance probe (Varian Inc, Palo Alto, CA). Experiments were run at 298 K by using standard pulse sequences as supplied as part of the Varian protein pack. Data collection included 1024 t_3 points, 24 t_2 points, and 64 t_1 points, subsequently extended with linear prediction and zero filling to 2048, 64, and 128 points, respectively.

The ^{31}P spectra used for analysis of nucleotide content were collected on a Mercury 300-MHz spectrometer, with a Nalorac 4 nucleus probe, using standard one-dimensional experiments having proton decoupling only during acquisition. Relatively long recycle times of 2 s were selected to minimize variations in peak intensities due to differential spin relaxation. ^{31}P chemical shifts were externally referenced to 85% phosphoric acid and internally referenced to 10 mM inorganic phosphate from sample buffer (pH 7.0).

The in-phase anti-phase ^1H-^{15}N HSQC experiments used to measure RDCs were adapted from a pulse sequence described previously (26) and run under both isotropic (288 K) and partially aligned (303 and 301 K) conditions on both ether bicelle and C_8E_5 samples. Data collection for the in-phase anti-phase ^1H-^{15}N HSQC experiments typically included 1024 t_2 points and 256 t_1 points, subsequently extended with linear prediction and zero filling to 2048 and 1024 points, respectively. Differences in the splittings from both aligned and isotropic conditions (303 K (ether bicelle)/301 K (C_8E_5) and 288 K (both)) yielded residual dipolar couplings.

^1H-^{15}N Cleanex HSQC experiments were used to identify amide protons that rapidly exchanged with protons from water in both full-length and Δ17Arf1·GDP samples. Experiments were adapted from a pulse sequence described previously (27) and conducted on samples made to be 0.5 mM protein in the aforementioned potassium phosphate buffer. Data collection for the Cleanex ^1H-^{15}N HSQC experiments included 2048 t_2 points and 128 t_1 points subsequently extended with linear prediction and zero filling to 4096 and 512 points, respectively. Data processing, including extraction of residual dipolar couplings, was performed with the nmrPipe/nmrDraw package (28); spectral figures were generated with the NMRview graphics package (29), and molecular graphics were generated using the Pymol Molecular Graphics package (DeLano Scientific, San Carlos, CA).

RDC Analysis and Back Calculation—Experimental dipolar couplings were initially analyzed using the REDCAT analysis package to allow an evaluation of a principal order frame and order parameters (30). Upon obtaining the assignments of the ^{15}N-^1H cross-peaks for Δ17Arf1·GDP, elements of the alignment tensor were found by analysis of couplings from 40 assigned peaks in the structurally conserved region. Principal order parameters using Arf1·GDP (or Δ17Arf1·GTP) crystal coordinates obtained from the above analysis are as follows for ether bicelles: S'_{xx}, S'_{yy}, and S'_{zz} = 0.00012, 0.00004, and −0.00016 (0.00009, 0.00003, and −0.000093); Euler angles relating the principal order frame to the molecular frame of the crystal structure are α, β, γ = −83, 86, and 50 (−56, 233, and 34). The corresponding parameters for the C_8E_5 medium were found to be S'_{xx}, S'_{yy}, and S'_{zz} = 0.00042, 0.00006, and −0.00048 (0.00026, 0.00010, and −0.00036) and α, β, γ = −44, 85, and 119 (−29, 54, and 122). Residual dipolar couplings were back-calculated for all ^{15}N-^1H vectors in both crystal structures (Arf1·GDP and Δ17Arf1·GTP) by using alignment and derived order tensor ele-

ments. These couplings, which ranged from −6 to 6 Hz (ether bicelle) and −13 to 15 Hz (C_8E_5), were compared with experimental couplings to provide an initial evaluation of the similarity of Δ17Arf1·GDP to these structures.

Structure Refinement against Dipolar Restraints—Refinement of existing crystal structures for Arf1·GDP, modified by removing the N-terminal helix coordinates, and Δ17Arf1·GTP was performed using the standard energy functions (bond, angle, improper, Van der Waals, and electrostatic) and RDC constraint functions (sani) in the XPLOR-NIH package (31). Both starting structures included the bound nucleotide, the coordinated magnesium ion, and explicit water molecules. Refinement made use of a combination of torsion angle minimization (IVM module (32)) and Powell minimization in Cartesian space as described in the literature (33). The latter was used to allow full adjustment in position of all atoms, represented as small departures from idealized covalent geometry, in response to the RDC constraints as described below (see "Protocol Validation"). There has been concern that undesired distortion of peptide plane geometry might occur in response to application of RDC constraints on H-N bond vectors using solely Cartesian methods, making torsion or rigid body minimization a preferred procedure. However, it is widely recognized that modest (≤6°) departures from ideal peptide plane geometry can be the result of the local environment within proteins (34), and suppression of these expected variations might force compensation in backbone torsion angles upon refinement. As this would lead to a greater degree of ϕ and ψ angle variation, refinement first in torsion angle space followed by short rounds of Cartesian minimization was chosen. The force constants for bonds and angular components (angles and improper torsions) were set to 1000 kcal mol^{-1} $Å^2$ and 500 kcal mol^{-1} rad^2, respectively (33), resulting in peptide bond distortions well within the expected range (average deviation from planarity of 1.7° and maximum deviation of 6°). Forces used with RDC constraints were adjusted in order to bring agreement between experimental and back-calculated RDCs only within experimental error.

In order to incorporate RDC constraints into energy minimization refinement, pseudo-atoms *X*, *Y*, *Z*, and *O* representing the tensor orientation in each alignment frame were first added to the starting coordinates. These pseudo-atoms were held rigid with respect to one another but allowed rotational degrees of freedom centered on *O* during refinement. Harmonic well potentials were then added for RDC data (E_{SANI}) along with values of dynamic frequency shift, Da ($(1/2)S_{zz}$), and rhombicity of 0.0 (0.0), −19.55 (−17.45), 0.51 (0.33), for C_8E_5 and ether bicelle data, respectively.

Minimization progressed using the following schedule. Initial Powell minimization was first carried out in Cartesian space (no dipolar restraints) until convergence. Powell minimization in torsion angle space was then implemented followed by short rounds of Cartesian space minimization with RDC force constants increasing linearly over 500 steps to their final values (2.0 (ether bicelle) and 1.0 (C_8E_5)) by using 1000 rounds of minimization at each step. Finally, Cartesian minimization (500 steps; no RDC restraints) was carried out to allow for return to ideal covalent geometry, and Powell minimization in torsion angle space, with RDC forces set to their final values for 750 rounds, was used to allow for RDC convergence without disrupting peptide plane geometry. A typical minimization schedule required 2 h on a dual 2.8-GHz Intel xenon system with 2 gigabytes of RAM.

The degree of correlation between refined structures and back-calculated data was expressed as both the root mean square deviation (r.m.s.d. in Hz) of data from the best fit correlation line and the Quality factor (Q) (35), defined in Equation 3,

$$Q = \text{r.m.s.}(D^{calc} - D^{obs})/\text{r.m.s.}(D^{obs}) \quad \text{(Eq. 3)}$$

where D^{obs} and D^{calc} are observed and calculated one-bond dipolar couplings, respectively.

The precision of the refinement scheme was examined by conducting 10 separate calculations having left out separate 10% fractions of the dipolar data. This was done as an attempt to generate alternate minimization trajectories during refinement. All structures produced agree to within 1.0 Å r.m.s. deviation of Cα positions when compared with structures generated using all available dipolar data. These structures are being separately deposited (Protein Data Bank code 1U81). However, the small variation in overall structures adds confidence to observed deviations from the starting model to be discussed below.

Protocol Validation—Residual dipolar couplings were simulated from three coordinate files (1HUR (Arf1), 1D3Z (rubredoxin), and 1BQ8 (ubiquitin)) obtained from the Protein Data Bank. The structures were allowed to relax using XPLOR-based constant temperature (C_T) dynamics simulations for 20 ps at 500, 1000, 1500, and 2000 K (10 ps), which yielded structures with Cα atoms that had r.m.s. deviations from starting models of 0.8, 1.2, 2.2, and 3.1 Å, respectively. Energy minimization refinement was attempted on these model structures using solely Cartesian-based, solely torsion-based, or combined methods as described previously (initial minimization with no RDC constraints, minimization with linearly increasing RDC forces, and final minimization) using H-N residual dipolar couplings simulated from two independent alignment frames ($S_{zz} = 6.9e^{-4}$ and $\eta = 0.31$ (RDC 1), and $S_{zz} = -1e^{-3}$ and $\eta = 0.19$ (RDC 2)).

The effectiveness of the refinement protocol was determined by comparing Cα r.m.s. deviations and RDC correlations between starting (1HUR, 1D3Z, and 1BQ8) and minimized models. Powell minimization relying solely on torsional degrees of freedom only returned backbone coordinates to within 1-Å r.m.s. deviation in models relaxed to 2.2 Å (C_T 1500 K, 20 ps) with 3.2-Hz ($Q = 21\%$) agreement of simulated RDCs. Deviations in backbone atoms are in this case largely the result of translational differences in secondary structural elements and loop regions. Powell minimization in Cartesian space (with modifications to the topology file converting dihedrals defining planarity to impropers) allowed for 2.3-Hz RDC correlation ($Q = 15\%$) and an ability to return models relaxed to 3.1 Å (C_T 2000 K, 10 ps) to within 1 Å of the starting structure in all cases attempted. It is important to note that the major deviations in backbone positions observed in Cartesian minimization are found in loops, and those that correspond to secondary structural elements show deviations less than 0.6 Å. The translational deviations observed in torsion angle minimization are absent when minimizing in Cartesian space. It is likely that the smaller set of variables available in torsion angle minimization leads to a more restricted path over the energy landscape and more difficulty in returning to the initial structure. By using a combined torsion angle, Cartesian approach as described above allows for an improved level of convergence over both approaches based on Cartesian minimization and torsion minimization alone. This approach showed an ability to refine structures relaxed to 3.1 Å to *less than* 1-Å r.m.s. deviation when compared with starting structures (1HUR, 1D3Z, and 1BQ8) and allowed for 1.98 Hz ($Q = 13\%$) agreement between dipolar couplings. Hence, the combined approach was chosen for application to Arf1 structures.

RESULTS

Qualitative Assessment of Conformational Change as a Result of Truncation—If most structural alterations in the Arf1 molecule were dependent solely on nucleotide exchange, we would anticipate the closest structural homolog of Δ17Arf1·GDP to be Arf1·GDP. We therefore begin our presentation with a qualitative comparison of these two molecules. As mentioned previously, the N-terminal helix of Arf1·GDP lies in a cleft parallel to the C-terminal helix (αCt) located opposite the nucleotide-binding site. One might expect that the N-terminal helix could be removed with minimal perturbation to most parts of the molecule, except for possible perturbations to the nearby αCt-helix and portions of the ISR found near the N-terminal helix, and that this structure, with the helix removed, would serve as a good model for Δ17Arf1·GDP (in which the nucleotide is unchanged). Indeed, it has been reported that a crystal structure for Δ17Arf1·GDP determined with coordinates little changed from those of Arf1·GDP (8).

^1H-^{15}N heteronuclear single quantum coherence (HSQC) spectra are often used as a fingerprint for structural characteristics of soluble proteins. Positions of cross-peaks are sensitive to a combination of amino acid type and local structural alterations (36, 37). If structure was preserved between Arf1·GDP and Δ17Arf1·GDP except for N-terminal helix deletion, HSQC spectra should superimpose with primary differences being the absence of peaks for the N-terminal 17 residues and shifting of peaks for residues belonging to the C-terminal helix. Overlaying the ^1H-^{15}N HSQC spectra for these molecules shows differences that are extensive (Fig. 2). Analysis of the differences that do exist requires peak assignment for both spectra. Assignments for Arf1·GDP have been reported previously (38). Assignments for Δ17Arf1·GDP were carried out by using triple resonance methods as described under "Experi-

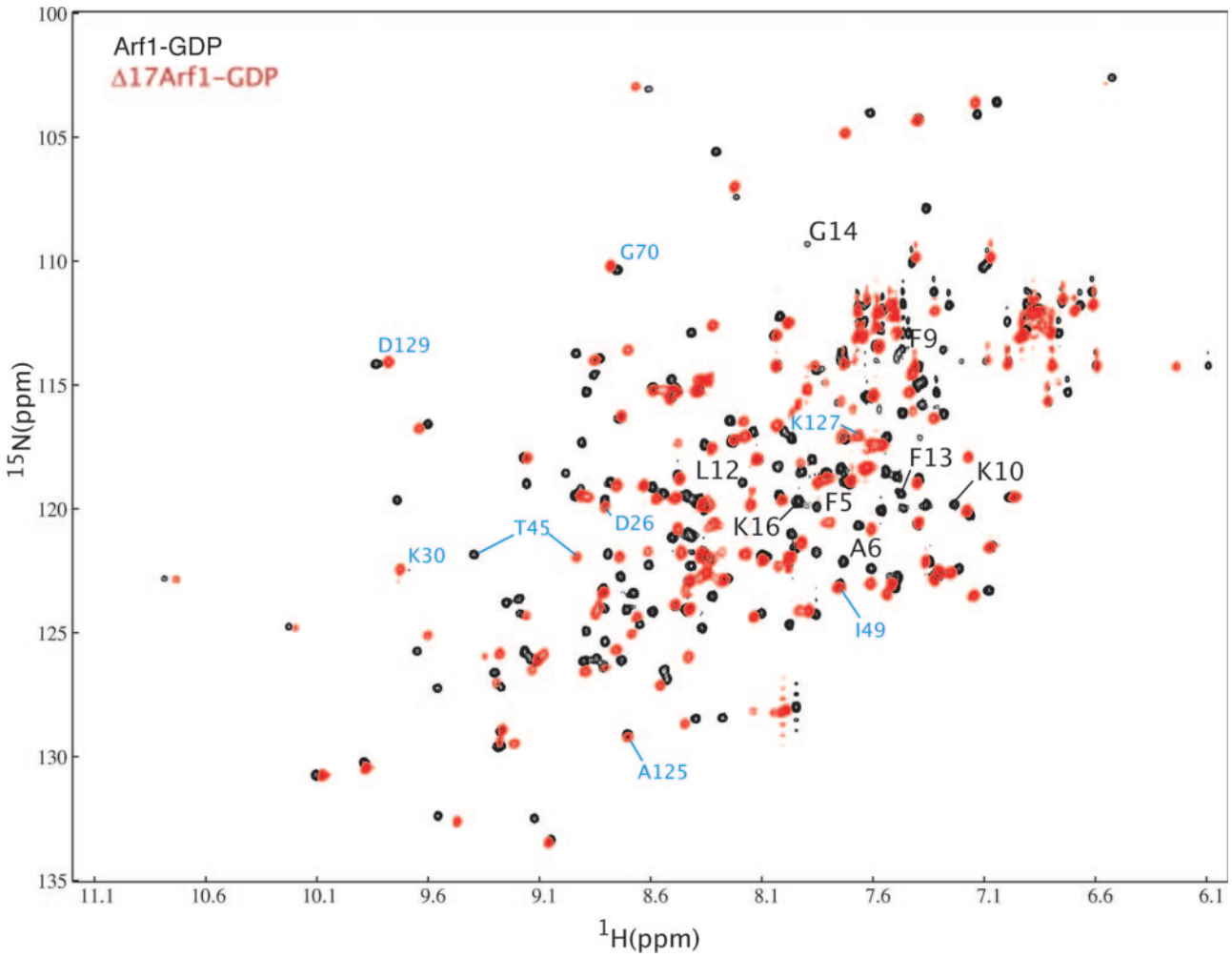

FIG. 2. **Overlay of the ^{1}H, ^{15}N-HSQC spectra of 0.5 mM Arf1·GDP (*black*) on spectra of Δ17Arf1·GDP (*red*) both in 10 mM phosphate buffer (pH 7.0).** Spectra recorded at 298 K with a ^{1}H resonance frequency of 800 MHz. Residues of the N-terminal α-helix found in Arf1·GDP not present in Δ17Arf1·GDP are labeled in *black*. Residues found within the nucleotide-binding pocket (P-loop (Asp-26 and Lys-30) and G3Motif (Ala-125, Lys-127, and Asp-129)) are labeled in *light blue* and are considered representative peaks with little expected variation between models. Most interestingly, those of SW1 (Thr-45) show a large degree of chemical shift variance.

mental Procedures." These assignments are reported in the Supplemental Material and have been deposited in the Protein Data Bank (1U81). Representative cross-peaks for Arf1·GDP that have shifted or lack obvious counterparts in Δ17Arf1·GDP are summarized in Table II. Residues found within the nucleotide-binding pocket (P-loop (Asp-26 and Lys-30) and the G3Motif (Ala-125, Lys-127, and Asp-D129)) are also labeled and considered representative peaks with little expected variation between models. Peaks that exhibit significant shifts are in fact distributed throughout the structure (illustrated in Fig. 2 and summarized in Table II).

Qualitative Assessment of Conformational Change as a Result of Nucleotide Exchange—Given these differences, we must also examine the possibility that most differences seen between Arf1·GDP and Δ17Arf1·GTP crystal structures are actually triggered by truncation, and that the Δ17Arf1·GTP crystal structure may be a better model for Δ17Arf1·GDP. This would result in a greatly expanded list of peaks that deviate in comparing HSQC spectra of Δ17Arf1·GDP and Arf1·GDP. Peaks might include residues near SW1, SW2, and the interswitch region, as well as residues in contact with the nucleotide-binding site. As discussed in the Introduction, conformations in these regions deviate significantly between structures. Several residues in the suggested regions do shift as labeled on the HSQC overlay of Fig. 2 and in the list of Table II. However, an equal number do not, specifically members of the phosphate-binding loop and a few members of the guanine base binding motif labeled in Fig. 2 (P-loop (residues 26–30) and G3Motif (residues 126, 127, 129), respectively).

If one were to propose that Δ17Arf1·GTP might provide a better structural homolog to Δ17Arf1·GDP, one might also expect their HSQC spectra to superimpose with possible perturbations within residues found solely in the nucleotide-binding pocket. However, upon overlaying HSQC spectra obtained for Δ17Arf1·GDP and Δ17Arf1·GTP (Fig. 3), variations in chemical shifts are far more numerous than the number that might be expected to surround the binding pocket; specifically, those of both SW1 (Thr-45 and Ile-49) and SW2 (Gly-70) also show a large degree of chemical shift deviation. This suggests that neither of the two crystal structures are a good model for Δ17Arf1·GDP, allowing for the possibility that Δ17Arf1·GDP is a structural intermediate between the two states.

Residual Dipolar Coupling Comparison and Structure Refinement—A more direct measure of structural change lies in residual dipolar coupling measurements. Here we compare experimentally measured N-H RDCs to predictions based on directions of N-H bond vectors seen in the crystal structures of Δ17Arf1·GTP and Arf1·GDP. Calculation of predicted couplings for comparison to structural models requires an initial evaluation of order parameters from experimental data. This in turn

TABLE II
Chemical shift differences between Arf1·GDP and Δ17Arf1·GDP

The abbreviations used are as follows: Nt, N-terminal helix; Ct, C-terminal helix; SW1, switch 1 region; SW2, switch 2 region; ISR, inter-switch region. Residues shown are representatives found in secondary structural regions having either no currently identified partner peak (labeled NP) or a significant degree of shift. Unexpected shifts are in boldface.

		Chemical shift assignments (ppm)			
		Arf1·GDP		Δ17Arf1·GDP	
		^{1}H	^{15}N	^{1}H	^{15}N
Nt	Phe-5	7.85	119.9	NP	NP
Nt	Ala-6	7.67	120.6	NP	NP
Nt	Phe-9	7.49	113.9	NP	NP
SW1	**Val-43**	**9.12**	**132.5**	**NP**	**NP**
SW1	**Thr-44**	**8.90**	**126.1**	**NP**	**NP**
SW1	**Thr-45**	**9.39**	**121.8**	**8.94**	**120.1**
SW1	**Ile-46**	**8.42**	**122.3**	**8.34**	**120.8**
ISR	**Asn-52**	**7.73**	**122.1**	**7.46**	**116.1**
ISR	**Val-53**	**8.89**	**124.9**	**8.68**	**118.3**
ISR	**Glu-54**	**8.81**	**126.4**	**8.29**	**120.4**
ISR	**Val-56**	**8.61**	**122.2**	**NP**	**NP**
ISR	**Lys-59**	**8.74**	**122.7**	**8.02**	**115.2**
SW2	**Gly-70**	**8.75**	**110.3**	**8.77**	**108.8**
SW2	**Gln-71**	**8.54**	**119.4**	**8.56**	**118.1**
Ct	Leu-170	8.42	121.1	8.30	119.2
Ct	Asn-179	7.47	116.1	7.42	113.9
Ct	Gln-180	7.56	120.0	7.47	117.2

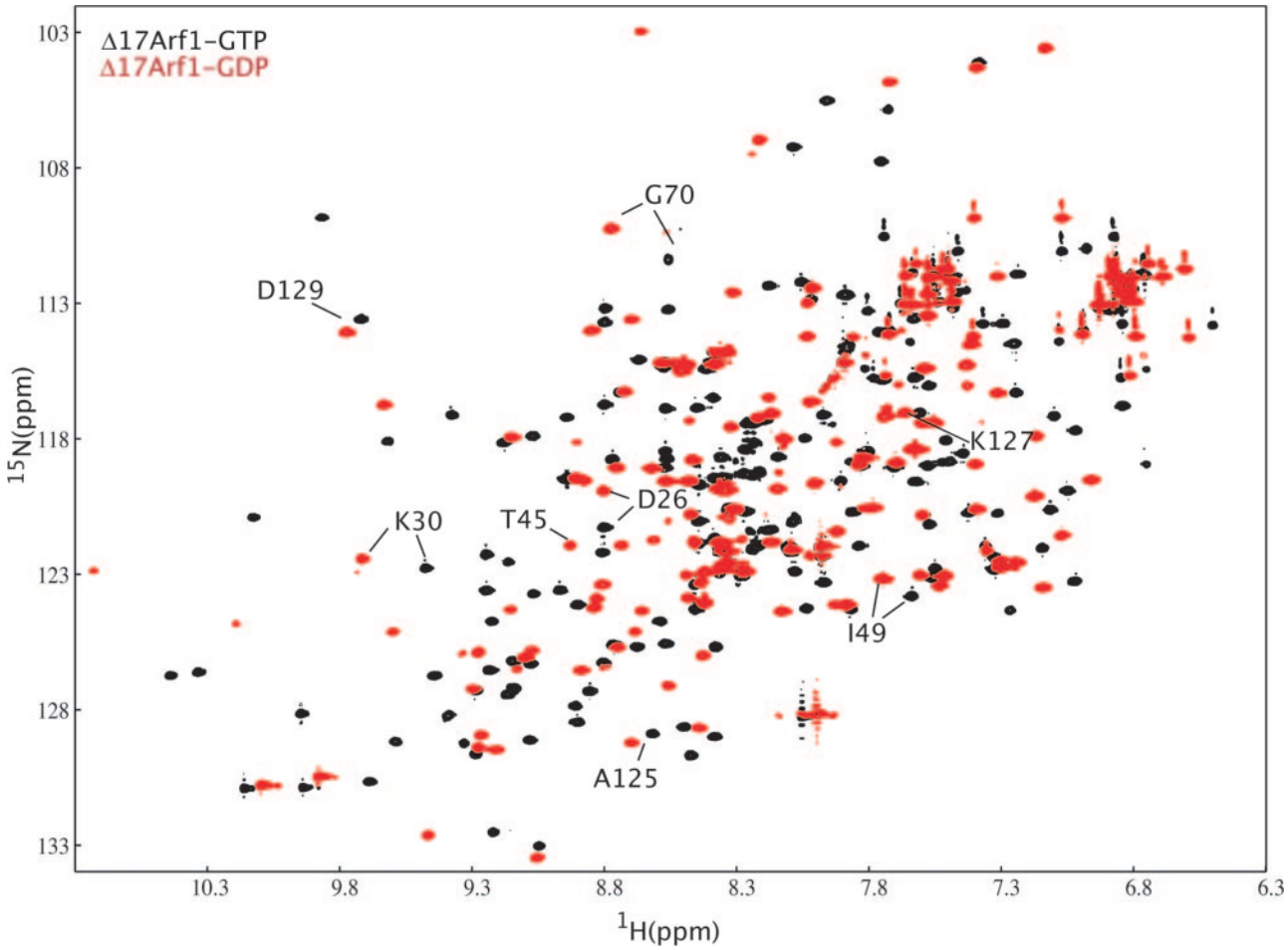

FIG. 3. **Overlay of the ^{1}H, ^{15}N-HSQC spectra of 0.5 mM Δ17Arf1·GTP (*black*) on spectrum of Δ17Arf1·GDP (*red*) each in 10 mM phosphate, pH 7.0.** Spectra were recorded at 298 K with a ^{1}H resonance frequency of 800 MHz. Residues found within the nucleotide-binding pocket (P-loop (Asp-26 and Lys-30) and G3Motif (Ala-125, Lys-127, and Asp-129)) are labeled in *black* and are shown as representative peaks with a higher degree of expected variation between models. Those of both SW1 (Thr-45 and Ile-49) and SW2 (Gly-70) also show a large degree of chemical shift deviation.

requires a conserved structural segment within the molecules to be identified.

Comparing crystal structures for Arf1·GDP and Δ17Arf1·GTP reveals residues 90–165 as structurally conserved (*e.g.* see Fig. 1, shown in neutral tones). Major structural differences are restricted to β-strands 1–3, including both

switch regions and the connecting loops as described (8) and illustrated in Fig. 1 above. We have used data from the structurally conserved segment to determine order parameters, and we used these order parameters to back-calculate other expected couplings.

Because there are always minor structural variations between proteins in solution and those in crystals, it is important to calibrate this back-calculation procedure on a system where structural homology is expected to be high. Comparing the measured residual dipolar couplings for Arf1·GDP to those predicted from the crystal structure of the same molecule should set the expected level of agreement (base line) between a well defined structure in solution and its crystal counterpart. By using 37 dipolar coupling values in the most conserved region, an order tensor for Arf1·GDP in a bicelle medium was calculated. All couplings were then back calculated by using these order parameters along with atomic coordinates from the full-length crystal structure (11).

A correlation plot of experimental and back-calculated RDC data for Arf1·GDP is presented in Fig. 4*A*. This shows a strong correlation between measured and experimental values having a root mean square deviation of 5 Hz. This corresponds to deviations that are somewhat larger than experimental precision (2 Hz), but the structural variations leading to this deviation can be quite small. An alteration of 10° in the average orientation of an N-H vector, if near a direction of optimal sensitivity in a molecule ordered to the extent observed here, would produce a change in dipolar coupling of 5.2 Hz. There are also a few outliers in the plot. These correspond to residues in loops (Leu-25 and Ala-27 (P-loop); Lys-129 and Asn-135 ($L\beta_{5/\alpha D}$); Gln-180 and Lys-181 (C terminus)) whose structure might be expected to deviate more between solution and crystal. Remaining deviations above 2 Hz correspond to small adjustments in local N-H vector angles.

Refinement of the structure through an energy minimization regime consisting of Powell minimization in torsion angle space followed by short rounds of Powell minimization in Cartesian space (see "Experimental Procedures"; hereafter referred to as torsion angle minimization) can make these small adjustments without significant changes in backbone structure. By using an RDC force constant of 2, the r.m.s.d. between experimental and back-calculated couplings reduced to below the expected experimental precision (2 Hz); the associated quality factor (Q) for this refined structure is 13% (see "Experimental Procedures"). The resulting correlation plot is shown in Fig. 4*D*. The backbone Cα atom positions of the resulting molecular structure have an r.m.s.d. from those in the starting structure of 0.8 Å, largely due to movement of SW2 loop residues from the starting crystal structure (1HUR); these residues were determined previously to have a high B factor (11). Removing these residues from the r.m.s.d. comparison reduces the corresponding Cα deviation to 0.5 Å.

Comparison of experimental residual dipolar coupling data for Δ17Arf1·GDP to coupling data predicted from the Arf1·GDP structure can now be undertaken. This should give an experimental view of changes induced by truncation without the complication of simultaneous nucleotide exchange. In this case data from two different media were available, greatly improving an ability to assess structural differences. Elements of the alignment tensor in these two media, ether bicelles and C_8E_5: octanol (C_8E_5), were found by using residual dipolar coupling data for 40 assigned peaks in the structurally conserved region and the Arf1·GDP crystal coordinates (all measured RDCs are given in the Supplemental Material). It is important to note that the overall range of dipolar couplings found for Δ17Arf1·GDP is smaller than that of Arf1·GDP due to a smaller degree of alignment in the liquid crystal media (−6 to 6 Hz in ether bicelle media and −13 to 15 Hz in C_8E_5 media as compared with −30 to 31 Hz for Arf1·GDP in bicelle media). Therefore, in what follows, couplings of Δ17Arf1·GDP have been scaled to match the range of dipolar couplings originally observed for Arf1·GDP to facilitate direct comparison.

A correlation plot of experimentally measured values for Δ17Arf1·GDP in ether bicelle and C_8E_5 media *versus* predicted values based on the Arf1·GDP crystal structure is shown in Fig. 4*B*. This shows a modest correlation between measured and predicted values having scaled r.m.s.d. of 9.9 and 9.7 Hz, respectively (Q = 86%). However, the agreement is significantly less than in the Arf1·GDP solution to crystal comparison given above. Again, torsion angle refinement of the Arf1·GDP coordinates against RDC constraints using a force constant adjusted to compensate for the change in RDC range can impose a greater degree of correlation between dipolar values and, in fact, reach a value within experimental precision (r.m.s.d. of 3.4 Hz (Q = 33%), Fig. 4*E*). However, in this instance backbone torsion angles were significantly modified as a result of refinement. The r.m.s.d. of the Cα backbone atom positions relative to the starting structure was 2.5 Å.

Comparison of experimental RDC data for Δ17Arf1·GDP to coupling data predicted from the structure of Δ17Arf1·GTP should give a representation of changes induced by nucleotide exchange. A correlation plot of experimentally measured *versus* predicted values is shown in Fig. 4*C*. This shows a very poor correlation between measured and predicted values, having an overall scaled r.m.s.d. of 12.3 Hz (Q = 103%). In principal a refinement of this structure (Δ17Arf1·GTP) should lead to the same refined structure as that obtained starting from Arf1·GDP. Refinement of the Δ17Arf1·GTP coordinates against RDC constraints using the same force constant given above, in this instance, does not improve the correlation between dipolar values (Fig. 4*F*, r.m.s.d. 13.0 Hz (Q = 107%)). This type of behavior is not unexpected in a minimization routine when conversion between structures would involve substantial energy barriers. Simulated annealing protocols (31, 39) offer a possibility for overcoming these barriers under circumstances where both translational and orientational degrees of freedom are restricted, but with only N-H RDC restraints these methods prove unproductive (40). We can, however, conclude that the structure of Δ17Arf1·GDP must deviate more from the Δ17Arf1·GTP crystal structure than from that of Arf1·GDP.

Additional Information Relating Truncated and Nontruncated Arf1 Structures—NOE data can confirm some of the similarity between the Δ17Arf1·GDP structure in solution and the Arf1·GDP crystal structure. ^{15}N-edited HSQC-NOESY experiments involving Δ17Arf1·GDP and Arf1·GDP were collected by using a mixing time of 150 ms on samples similar to those used for the RDC experiments except for the absence of alignment media. These data are rather limited because only NOEs involving amide protons are detected, and cross-peaks only to assigned resonances along the backbone can be identified. However, assigned NOEs in some critical regions do occur. In particular, the amide proton from methionine 22 (β1) in Δ17Arf1·GDP shows a weak NOE connectivity with the α-proton from valine 64 (β3). This bridges β-strands involved in the interswitch hydrogen bond network. The same contact is seen in Arf1·GDP, suggesting this portion of the interswitch remains intact (data not shown).

Another set of data easily accessed through assigned ^{15}N-^{1}H HSQC spectra is amide proton exchange rates. A commonly used model assumes that the amide group is in rapid equilibrium between occluded and exposed forms with base-catalyzed

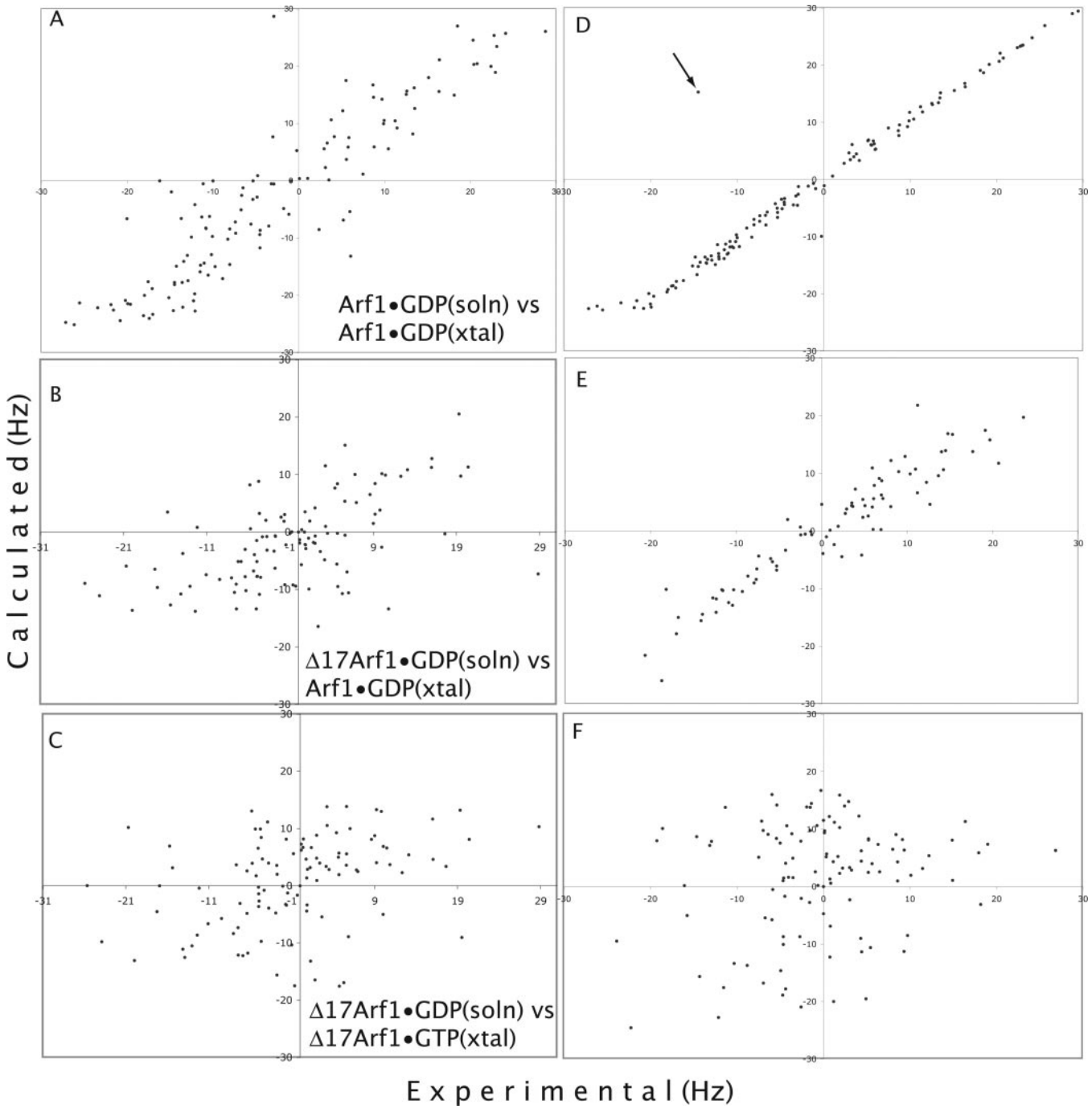

FIG. 4. **Correlation plot of experimentally measured ^{15}N-^{1}H dipolar couplings *versus* those calculated from unrefined crystal coordinates for Arf1·GDP (experimental) *versus* Arf1·GDP(calculated) (*A*); Δ17Arf1·GDP (experimental *versus* Arf1·GDP (calculated)) (*B*), and Δ17Arf1·GDP (experimental) *versus* Δ17Arf1·GTP (calculated) (*C*).** In all cases, the *x* axis denotes experimentally measured couplings, and the *y* axis denotes calculated couplings from the specified crystal coordinates. The degree of correlation is expressed as both a root mean square deviation in hertz of observed scatter and the quality factor (*Q*) as defined under "Experimental Procedures." The scatter seen in plots *A–C* indicates strong, modest, and poor levels of correlation between experimental couplings and those predicted from model structures having a resulting r.m.s.d. of 5, 9.7, and 12.3 Hz and associated quality factors of 44, 86, and 103%, respectively. These measured RDCs also show an ability to refine to convergence using torsion angle energy minimization when using Arf1·GDP as the starting model (*D* and *E*), having a resulting refined r.m.s.d. of 1.75 and 3.4 Hz, respectively (Q = 13 and 33%). When using Δ17Arf1·GTP coordinates in refinement, the RDC correlation showed no improvement (*F*) with a corresponding r.m.s.d. of 13 Hz (Q = 107%). The outlier denoted by an *arrow* is from residue 70, omitted from energy minimization refinement due to a high *B* factor in the starting model.

exchange of the amide proton for a water proton in the open form being the rate-limiting step (41). Under these conditions, increases in rates of exchange reflect primarily destabilization of occluded forms and a shift in equilibrium toward conformations that expose amide protons to solvent. Normally, rates are measured by monitoring decreases in HSQC peak intensities as amide protons are replaced by deuterium from deuterated water added to the sample. When rates of interest are fast, however, an equivalent experiment can be conducted in which water protons are labeled by saturation or inversion of magnetization. Differences between spectra with water magnetization perturbed and not perturbed highlight cross-peaks belonging to amides experiencing rapid proton exchange. The CLEANEX HSQC is an experiment of this class that has been

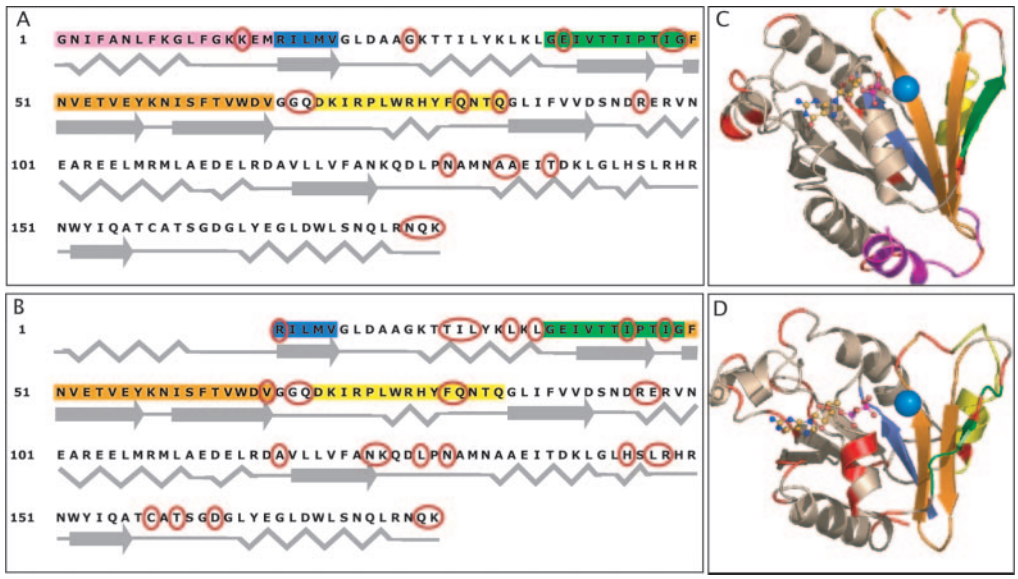

FIG. 5. ^{1}H-^{15}N Cleanex HSQC comparisons, showing areas of rapid exchange between water and amide protons of Arf1·GDP (*A*) and Δ17Arf1·GDP (*B*). Secondary structural elements are shown as a *schematic* below the one-letter amino acid code for the protein sequence. Resonances evident in a ^{1}H-^{15}N Cleanex HSQC experiment are *circled* in *red.* To relate these regions of enhanced exchange to a three-dimensional model, structures of Arf1·GDP (*C*) and Δ17Arf1·GDP (*D*) are shown as a schematic representation color-coded as follows: N-terminal α-helix (*magenta*), switch 1 (*green*), inter-switch β-strands (*orange*), and switch 2 (*yellow*); with Cleanex peaks represented as *red areas* in the respective three-dimensional models.

designed to minimize artifacts from inadvertent perturbation of α-protons underlying the water resonance (27). Here we present data on Arf1 proteins from the CLEANEX experiment.

Results for CLEANEX HSQC data for Arf1·GDP and Δ17Arf1·GDP are presented in Fig. 5, *A* and *B,* respectively. There are clearly more peaks in the Δ17Arf1·GDP case indicating an increase in exposed residues or destabilization of secondary structure elements that protect amide protons from exchange in Arf1·GDP. The amides showing rapid exchange have been mapped onto the sequences of the two proteins in Fig. 5, *C* and *D.* As expected, the majority of rapidly exchanging amides are in loops between secondary structure elements in both proteins. Major differences occur in the loss of some rapidly exchanging elements in the D-helix of Arf1·GDP on truncation and the addition of rapidly exchanging elements in helix A, the guanine-binding motif (G3Motif), and the loop immediately preceding the C-terminal helix in Δ17Arf1·GDP.

Quantitative Comparison of Conformational Change as a Result of Truncation—The best way to compare changes in Arf1 structure that might be induced by N-terminal truncation, as opposed to nucleotide exchange, is on the basis of a three-dimensional model of Δ17Arf1·GDP. Fortunately, torsion angle minimization of the Arf1·GDP crystal structure under RDC constraints collected on Δ17Arf1·GDP in solution did produce a modified structure. Torsion angle minimization schedules using 2 sets of dipolar restraints have shown an ability to converge RDCs (Q = 70% (start), Q = 13% (refined against simulated RDCs with no experimental error)) in structures having greater than 3-Å backbone r.m.s. deviation from starting models in test cases (see "Protocol Validation"). These tests also show an ability to return Cα backbone atoms from their initial 3-Å r.m.s. deviations to *less than* 1-Å r.m.s. deviation from the starting model, with most remaining deviations found in loop regions. Given that RDCs back-calculated from N-H bond vector positions in our Δ17Arf1·GDP model agree with both sets of experimental data within estimated precision (r.m.s.d. 3.4-Hz (Q = 33%)), this must be considered a valid structure.

The structure appears to be of reasonable quality. Examination of the structure using Procheck (42, 43) indicates that 69% of ϕ and ψ backbone angles fall within the most favored region of Ramachandran space, and an additional 29% fall within the acceptable region. There are no unacceptable bond angles or bond lengths. Because of the use of RDC constraints on N-H vectors to drive conformational changes, it was essential to examine N-H bond geometry in more detail. The out-of-plane distortions, as measured by Ω angles, are minimal (standard deviation of 1.7° and maximum deviation of 6°). These are comparable with deviations seen after minimization without RDC constraints (1.6 and 5.6°) and do not reflect unreasonable distortions due to RDC constraints. The same can be said for in-plane distortions as measured by HN-N-Ca bond angles (1.2 and 2° for the RDC constrained structure *versus* 1 and 1.8° for the unconstrained structure).

The model produced does not differ globally from the crystal structure of Arf1·GDP used as a starting point, as discussed below (2.5Å r.m.s.d. for backbone α-carbons). However, there are distinct regions that do differ. These are easily identified by looking at r.m.s. deviations as a function of residue number for Cα positions in superimposed structures for Δ17Arf1·GDP and the Arf1·GDP crystal structure. It is readily apparent that Cα positions differ not only in and around the switch regions but also throughout several other regions of the protein (Fig. 6). Among the regions showing the greatest degree of variation (r.m.s.d. > 2Å) are the switch regions, the interswitch strands, the C-terminal helix, and the now N-terminal β-strand (β1). Most surprisingly, residues involved in the nucleotide-binding pocket, specifically the nucleotide binding helix (αA), P-loop, and G3-binding motif, also show a large degree of Cα deviation. The model itself will be presented below.

DISCUSSION

Much like the original starting model (Arf1·GDP), the Δ17Arf1·GDP structure produced by refinement against dipolar couplings is composed of a mixed parallel/antiparallel 6 β-strand core surrounded by 5 α-helices and 12 connecting loops. However, SW1 now encompasses a much-diminished 7th antiparallel β-strand at the periphery of the core. As a direct result of removal of the N-terminal helix and connecting loop region, a multitude of small but global modifications have also occurred. Where these differences in structure are quite large

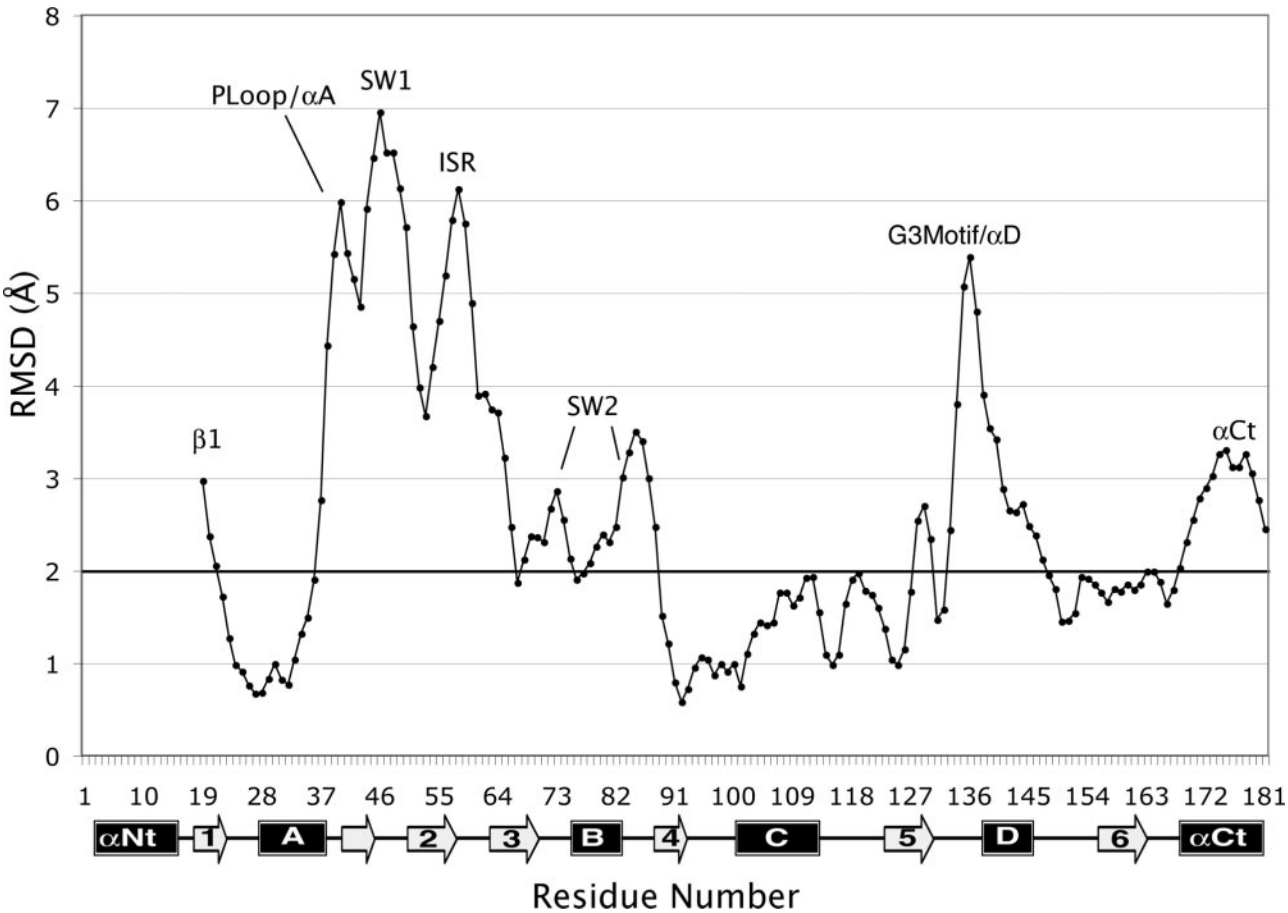

FIG. 6. **Root mean square deviation in angstroms seen upon overlaying the proposed Δ17Arf1·GDP solution structure with that of the starting model (Arf1·GDP), specifically overlaying β-strands 4–6 found predominantly unchanged in the protein core.** This highlights global deviations throughout the whole of the protein, ranging from 0.6 to 7 Å. Those deviations found significantly above these small global rearrangements (as denoted by a *horizontal black line* at 2.0Å) are labeled to correspond to regions shown in structure overlays of Fig. 7. The *x* axis denotes the residue number with corresponding schematic representations of secondary structure elements, and the *y* axis depicts r.m.s.d. in angstroms.

(2.0–5.7 Å), they can be readily detected in superimposed structures (illustrated in Fig. 7).

Most notably, the nucleotide-binding helix (αA) has adjusted its tilt allowing for a concerted shift in the coordinated magnesium ion (Fig. 7*A*). SW1, losing most of its extended sheet conformation, has both changed its pitch and its spatial location, propagating a spatial displacement within the interswitch β-strands, specifically residues 50–53 (β3) and 65–68 (β4), without a corresponding change in register (Fig. 7*B*). The nucleotide-binding pocket, shown in Fig. 7*C*, also shows a modest degree of structural variation. Specifically, displacement of P-loop residues causes closer contacts with the ribose of GDP, forcing a disengagement of the guanine base from specific contacts in the G3Motif. Finally, the C-terminal helix, because of a greater degree of conformational freedom, has now shifted its tilt toward the N-terminal binding cleft (Fig. 7*D*).

Some of the conformational adjustments indicated above can be further validated by using amide exchange data from the ^{1}H-^{15}N Cleanex HSQC experiment. In comparing the results shown in Fig. 5, *B–D*, the segments containing the largest number of rapidly exchanging residues are relegated to the secondary structural element αA, which appears to be destabilized (shown in Fig. 7*A*), the loop near the C terminus (158–163), which is also more exposed or destabilized after truncation, and the members of the G3Motif (Asn-126 and Lys-127), which have changed their association with the guanine base. It is interesting that all of these segments make direct contact with GDP or its associated Mg^{2+} ion in the Arf1·GDP crystal structure.

It has been suggested that all conformational differences between the two crystal structures illustrated in Fig. 1, *A* and *B*, result from the binding of GTP and not from truncation of Arf1. In support of this, Goldberg (8) reports, "the crystal structure of Δ17Arf1·GDP at 2.0 Å resolution closely resembles Arf1·GDP." This is largely true in the sense that secondary structural elements seen in Arf1·GDP are preserved in our solution structure of Δ17Arf1·GDP, and the difference in positions of common backbone atoms in the two structures have an overall r.m.s.d. of only 2.5 Å. Also, there is a much more significant deviation from the Δ17Arf1·GTP crystal structure; in fact, the description of structural changes in SW1, SW2, and interswitch regions on comparing our solution structure of Δ17Arf1·GDP to the crystal structure of Δ17Arf1·GTP would remain qualitatively the same as that already in the literature.

However, there are significant shifts of some of the elements and apparently energetically significant rearrangements of residues near the nucleotide-binding site on comparing our truncated Δ17Arf1·GDP structure to full-length Arf1·GDP. These shifts and rearrangements are apparently the source of the difference in chemical shift patterns seen in simple HSQC experiments when comparing Arf1·GDP to Δ17Arf1·GDP (Fig. 2). Moreover, they appear to be responsible for small adjustments in N-H vector directions that show up in residual dipolar coupling deviations distributed throughout the structure.

The structure produced by refinement against the dipolar couplings cannot in general be viewed as adopting some of the changes seen on comparing Δ17Arf1·GTP to Arf1·GDP. How-

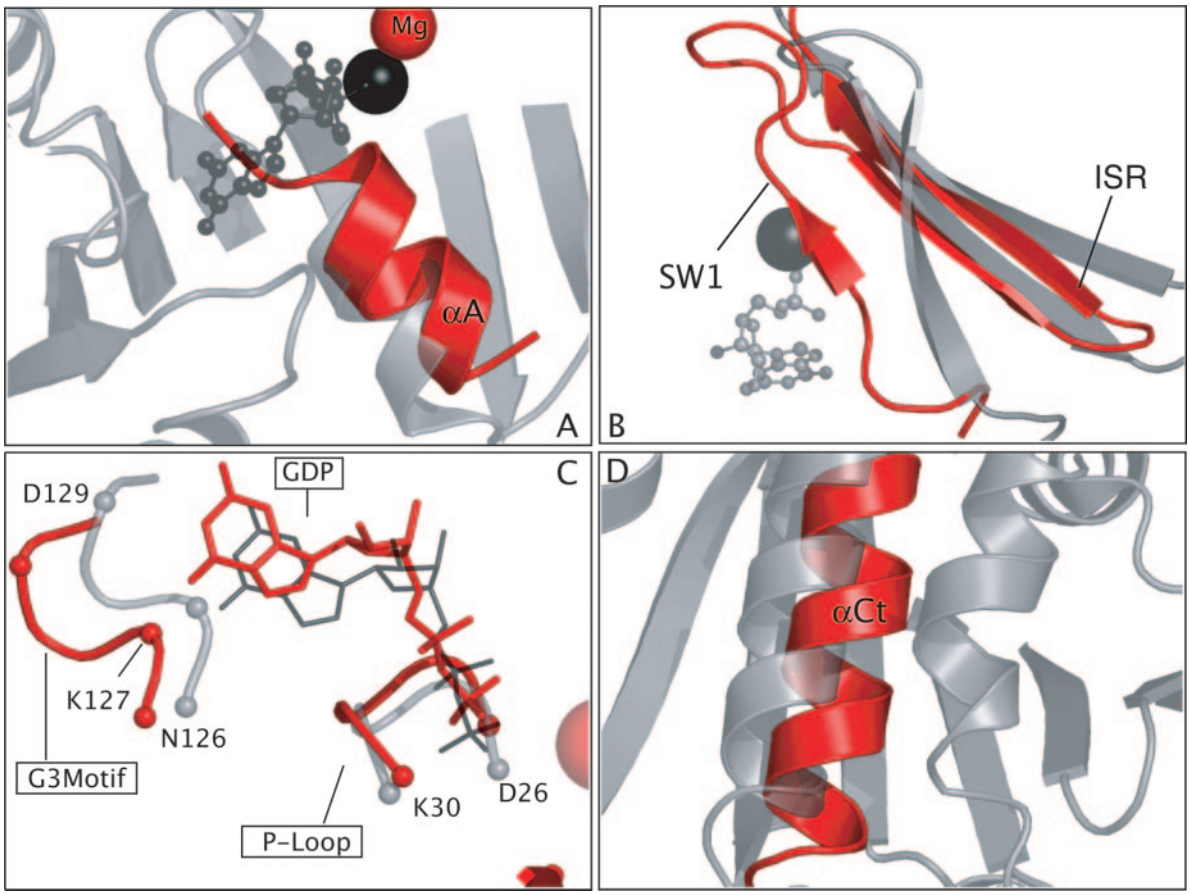

FIG. 7. **Superimposition of the proposed Δ17Arf1·GDP solution structure with Arf1·GDP using core β-strands 4–6 as anchor points.** In all cases darker colors (*gray* and *black*) indicate Arf1·GDP with *red* being representative of the proposed Δ17Arf1·GDP model. *A* shows a change in tilt of the nucleotide binding helix (*αA*) allowing for a concerted shift in the coordinated magnesium ion. SW1 (*B*), losing most of its extended sheet conformation, has changed its pitch and spatial location, propagating a displacement within the interswitch β-strands without a correlated change in register. The nucleotide-binding pocket, shown in *C*, shows displacement of P-loop residues causing closer contacts with the ribose of GDP and forcing a disengagement of the guanine base from specific contacts in the G3Motif. Residues directly involved in nucleotide coordination are labeled by amino acid type and residue number with respective Cα positions denoted by *spheres*. The C-terminal helix (*D*) has shifted toward the N-terminal binding cleft as a result of N-terminal truncation.

ever, the splaying and partial unraveling of the β-strand of SW1 and the changes in the ISR strands might be seen as movements along the path to complete unraveling of the SW1 β-strand seen in the crystal structure of Δ17Arf1·GTP. The Δ17Arf1·GDP solution structure we have produced is more appropriately viewed as a structural intermediate between the two crystal states.

The functional significance of our observations, including the destabilization observed for residues in contact with GDP in the binding site of Δ17Arf1, as compared with Arf1, and the shift in the position of the Mg^{2+} ion, may be connected with the altered nucleotide binding affinities of the truncated protein. It has been shown that truncated Δ17Arf1 has a higher affinity for GTP, whereas full-length Arf1 has a higher affinity for GDP. To the extent that truncation of the N-terminal helix mimics events that may happen on membrane association, these observations may be relevant to the effect of membrane association on nucleotide affinity. Despite early models that have Arf1 associating with membranes only in the GTP form, there is really little experimental evidence to support this; in fact, more recent models have begun to include association of the GDP-bound form (15, 20). If this is correct, the above data may indicate that membrane association actually promotes exchange of GDP for GTP. Association of guanine nucleotide exchange factors at the membrane surface may also be promoted by some of the changes seen. These factors are known to associate with residues at the surface of SW1. In our model, the extra strand provided by SW1 has moved in space potentially opening the protein to allow for subsequent association with its corresponding guanine nucleotide exchange factor. Hence, a model for structural reorganization upon contacting the membrane surface, prior to nucleotide exchange, is supported. Further structural studies on Δ17Arf1·GDP as well as Arf1·GDP in a phospholipid environment are needed to verify findings. Such studies should also allow tests of the structural and functional effects on Arf1 binding specific lipids, *e.g.* PI (4)P_1, PI(4,5)P_2, and phosphatidic acid.

Acknowledgments—We thank Dr. Homayoun Valafar, Dr. Andrew Fowler, Anita Kishore, and Dr. Catherine Bougault for their help throughout this project.

REFERENCES

1. Kahn, R. A., Yucel, J. K., and Malhotra, V. (1993) *Cell* **75,** 1045–1048
2. Shome, K., Vasudevan, C., and Romero, G. (1997) *Curr. Biol.* **7,** 387–396
3. Godi, A., Pertile, P., Meyers, R., Marra, P., Di Tullio, G., Iurisci, C., Luini, A., Corda, D., and De Matteis, M. A. (1999) *Nat. Cell Biol.* **1,** 280–287
4. Hill, K., Li, Y., Bennet, M., McKay, M., Zhu, X., Shern, J. F., Torre, E., Lah, J., Levey, A., and Kahn, R. (2003) *J. Biol. Chem.* **278,** 36032–36040
5. Takatsu, H., Yoshino, K., Toda, K., and Nakayama, K. (2002) *Biochem. J.* **365,** 369–378
6. Zhdankina, O., Strand, N. L., Redmond, J. M., and Boman, A. L. (2001) *Yeast* **18,** 1–18
7. Donaldson, J. G., Cassel, D., Kahn, R. A., and Klausner, R. D. (1992) *Proc. Natl. Acad. Sci. U. S. A.* **89,** 6408–6412
8. Goldberg, J. (1998) *Cell* **95,** 237–248
9. Pasqualato, S., Menetrey, J., Franco, M., and Cherfils, J. (2001) *EMBO Rep.* **2,** 234–238
10. Losonczi, J. A., Tian, F., and Prestegard, J. H. (2000) *Biochemistry* **39,** 3804–3816

11. Amor, J. C., Harrison, D. H., Kahn, R. A., and Ringe, D. (1994) *Nature* **372,** 704–708
12. Amor, J. C., Horton, J. R., Zhu, X., Wang, Y., Sullards, C., Ringe, D., Cheng, X., and Kahn, R. A. (2001) *J. Biol. Chem.* **276,** 42477–42484
13. Greasley, S. E., Jhoti, H., Teahan, C., Solari, R., Fensome, A., Thomas, G. M., Cockcroft, S., and Bax, B. (1995) *Nat. Struct. Biol.* **2,** 797–806
14. Kahn, R. A., Goddard, C., and Newkirk, M. (1988) *J. Biol. Chem.* **263,** 8282–8287
15. Franco, M., Chardin, P., Chabre, M., and Paris, S. (1996) *J. Biol. Chem.* **271,** 1573–1578
16. Zhu, X., Boman, A. L., Kuai, J., Cieplak, W., and Kahn, R. A. (2000) *J. Biol. Chem.* **275,** 13465–13475
17. Reinstein, J., Schlichting, I., and Wittinghofer, A. (1990) *Biochemistry* **29,** 7451–7459
18. Lacal, J., and McCormick, F. (eds) (1993) *The Ras Superfamily of GTPases*, CRC Press, Inc., Boca Raton, FL
19. Vetter, I. R., and Wittinghofer, A. (2001) *Science* **294,** 1299–1304
20. Renault, L., Guibert, B., and Cherfils, J. (2003) *Nature* **426,** 525–530
21. Prestegard, J. H., Al-Hashimi, H. M., and Tolman, J. R. (2000) *Q. Rev. Biophys.* **33,** 371–424
22. Bax, A., Kontaxis, G., and Tjandra, N. (2001) *Methods Enzymol.* **339,** 127–174
23. Neidhart, F. C., Bloch, P. L., and Smith, D. F. (1974) *J. Bacteriol.* **119,** 736
24. Griesinger, C., Otting, G., Wuthrich, K., and Ernst, R. (1988) *J. Am. Chem. Soc.* **110,** 7870–7872
25. Fesik, S. (1988) *Nature* **332,** 865–866
26. Wang, Y. X., Marquardt, J. L. Wingfield, P., Stahl, S., Lee-Huang, S., Torchia, D., and Bax, A. (1998) *J. Am. Chem. Soc.* **120,** 7385–7386
27. Hwang, T.-L., Mori, S., Shaka, A. J., and Zijl, P. C. M. V. (1997) *J. Am. Chem. Soc.* **119,** 6203–6204
28. Delaglio, F., Grzesiek, S., Vuister, G., Zhu, G., Pfeifer, J., and Bax, A. (1995) *J. Biomol. NMR* **6,** 277–293
29. Johnson, B., and Blevins, R. (1994) *J. Biomol. NMR* **4,** 603–614
30. Valafar, H., and Prestegard, J. H. (2004) *J. Magn. Reson.* **167,** 228–241
31. Schwieters, C. D., Kuszewski, J. J., Tjandra, N., and Clore, G. M. (2003) *J. Magn. Res.* **160,** 66–74
32. Schwieters, C. D., and Clore, G. M. (2001) *J. Magn. Reson.* **152,** 288–302
33. Clore, G. M., and Schwieters, C. D. (2004) *J. Am. Chem. Soc.* **126,** 2923–2938
34. MacArthur, M. W., and Thornton, J. M. (1996) *J. Mol. Biol.* **264,** 1180–1195
35. Cornilescu, G., Marquardt, J. L., Otiiger, M., and Bax, A. (1998) *J. Am. Chem. Soc.* **120,** 6836–6837
36. Kay, L. E., Keifer, P., and Saarinen, T. (1992) *J. Am. Chem. Soc.* **114,** 10663–10665
37. Stonehouse, J., Shaw, G. L., Keeler, J., and Laue, E. D. (1994) *J. Magn. Res.* **107,** 178–184
38. Amor, J., Seidel, R., Tian, F., Kahn, R., and Prestegard, J. (2002) *J. Biomol. NMR* **23,** 253–254
39. Tjandra, N., Omichinski, J., Gronenborn, A., Clore, G., and Bax, A. (1997) *Nat. Struct. Biol.* **4,** 732–738
40. Chou, J. J., Shipeng, L., and Bax, A. (2000) *J. Biomol. NMR* **18,** 217–227
41. Dempsey, C. (2001) *Prog. NMR Spec.* **39,** 135–170
42. Morris, A. L., MacArthur, M. W., Hutchinson, E. G., and Thornton, J. M. (1992) *Proteins* **12,** 345–364
43. Laskowski, R. A., MacArthur, M. W., Moss, D. S., and Thornton, J. M. (1993) *J. Appl. Crystallogr.* **26,** 283–291
44. DeLano, W. L. (2002) *The PyMol Molecular Graphics System*, DeLano Scientific, San Carlos, CA